JOURNAL OF GEOPHYSICAL RESEARCH, VOL. 101, NO. B11, PAGES 25,553–25,571, NOVEMBER 10, 1996

Tidal calibration of borehole strain meters: Removing the effects of small-scale inhomogeneity

R. H. G. Hart, M. T. Gladwin, and R. L. Gwyther

Division of Exploration and Mining, Commonwealth Scientific and Industrial Research Organisation Brisbane, Queensland, Australia

D. C. Agnew and F. K. Wyatt

Institute of Geophysics and Planetary Physics, University of California, San Diego

Abstract. We investigate the estimation of Earth strain from borehole strain meter data in a study of tidal calibration of the Gladwin borehole tensor strain meter (BTSM) at Piñon Flat. Small-scale geological inhomogeneity is one of several effects examined that cross couple remote areal/shear strain into measured areal/shear strain. A methodology is developed for incorporating cross coupling into the strain meter calibration. Using the measured strain tides from the colocated laser strain meter (LSM) as a reference, we show that calibration of the BTSM with cross coupling removes systematic errors of up to 30% in the borehole strain meter tides. This calibration accurately relates the BTSM measurements to strains at the scale length of the LSM, about 1 km. The calibration technique provides a solution to a major criticism of all short-baseline strain measurements, namely, that tectonic strains are not representatively sampled due to small-scale inhomogeneities. The technique removes errors potentially greater than 50% in observed strain offsets from fault slip, permitting improved constraint of slip mechanisms. We show that current theoretical estimates of strain tides in the instrument locality are not yet of sufficient accuracy for cross-coupled calibration. Comparison of theoretical tides with measurements from the LSM suggest that at least half of the error is in the ocean load tide estimates.

Introduction

Borehole strain meters [*Sacks et al.*, 1971; *Gladwin*, 1984] are a key component of worldwide earthquake/volcano hazard reduction programs, with some 100 instruments deployed in high hazard regions including California and Japan. The resolution (<1 $n\varepsilon$), bandwidth (~100 Hz to DC), and stability of the instruments permit most seismic and aseismic tectonic strain phenomena to be monitored. Observations of strain offsets help quickly and simply constrain the source mechanisms of earthquakes for a wide magnitude range [*Johnston et al.*, 1987; *Wyatt*, 1988; *Linde and Johnston*, 1989]. For many aseismic events strain meters provide the only constraints, as slip is generally too slow to excite appreciable seismic energy, and too fast and small to be detected by geodetic techniques [*Wyatt*, 1988]. Tensor borehole strain meters [*Gladwin*, 1984; *Sakata and Sato*, 1986] maximize the use of the expensive borehole installation by providing shear strains in addition to areal strain. The strains are obtained from three measurements, spaced 60° apart, of the radial deformation of a stainless steel cylinder grouted at 200 m depth in a vertical borehole [*Gladwin*, 1984].

Qualitative strain observations are of value to hazard reduction programs in, for example, detecting possible precursors, but maximum achievable accuracy of measurements is desirable for location and quantification of slip sources. Error reduction by averaging from many instruments in one locality is precluded by instrument and installation cost.

Accurate strain measurements require an accurate strain meter calibration relating instrument readings to Earth strains, but determination of this calibration is nontrivial. The instrument itself can be calibrated before installation, but instrument deformations do not directly reflect local strains. The borehole, the cement, and the instrument together form an inhomogeneity in the rock that distorts the strain field. There are two approaches to calibration. Direct estimation of elastic inclusion parameters has been used [*Gladwin and Hart*, 1985; *Shimada et al.*, 1987], but these parameters are difficult to determine and have large uncertainties. The preferred and more common approach is to use the instrument response to known reference strains for calibration. This procedure can be done at any time to check the stability of the instrument calibration in situ. The most accurately known reference signal is the Earth strain tide [*Harrison*, 1985].

The appropriate model of the coupling of Earth strain into the instrument should be incorporated in the calibration. *Gladwin and Hart* [1985] showed that, for an isotropic model of the instrument inclusion, the instrument areal strain equals the remote areal strain times a proportionality constant c, and the instrument shear strain equals the remote shear strain times a different proportionality constant d. The parameters c and d depend on the inclusion dimensions and elastic parameters, with typical values for the Gladwin strain meter (BTSM) of around 1.7 and 2.5, respectively.

Paper number 96JB02273.
0148-0227/96/96JB-02273$09.00

To calibrate under the assumption of isotropic coupling, the parameters c and d are determined from the ratios of the observed areal and shear strain tide amplitudes to corresponding theoretical strain tide amplitudes. This procedure was used to determine c for dilatometers [*Sacks et al.*, 1971; *Stefansson et al.*, 1981], and later extended to tensor instruments [*Gladwin et al.*, 1985]. While useful working calibrations have been obtained with this procedure, we now believe that it has limitations. In a calibration of the Piñon Flat BTSM using tides from the colocated laser strain meter, *Gladwin et al.* [1985] noted several discrepancies, particularly in shear tides, between calibrations obtained from different tidal constituents. These discrepancies were attributed at the time to instrument compass error and to tidal measurement errors. However, as shown below, a reevaluation with careful error analysis indicates that these explanations are inadequate.

It will be shown that effects such as small-scale geological inhomogeneity introduce cross coupling terms into the expressions relating remote strains to instrument strains. By cross-coupling we mean that an instrument strain component depends on all remote strain components rather than the single corresponding component of isotropic coupling. For example, instrument areal strain is a linear combination of remote areal and shear strains. Short baseline strain meters such as borehole strain meters are particularly vulnerable to the effects of small-scale geological inhomogeneity, as the spatial point sample from such instruments may not adequately represent the larger scale tectonic strains of interest. Small-scale inhomogeneity effects, of characteristic lengths 1 m to 1 km, were first identified by *Evans et al.* [1979] and have been seen in recent studies [*Kohl and Levine*, 1992; *Sato and Harrison*, 1990]. Cross-coupling effects were recognized by *Kohl and Levine* [1993] in borehole tiltmeter observations. Furthermore, the pervasive phenomenon in crustal rocks of elastic anisotropy of order 10% [*Crampin*, 1987; *Leary et al.*, 1990; *Jaeger and Cook*, 1979] is expected to produce cross-coupling terms of the same order, as discussed in Appendix A. Clearly, these effects need to be incorporated into calibration.

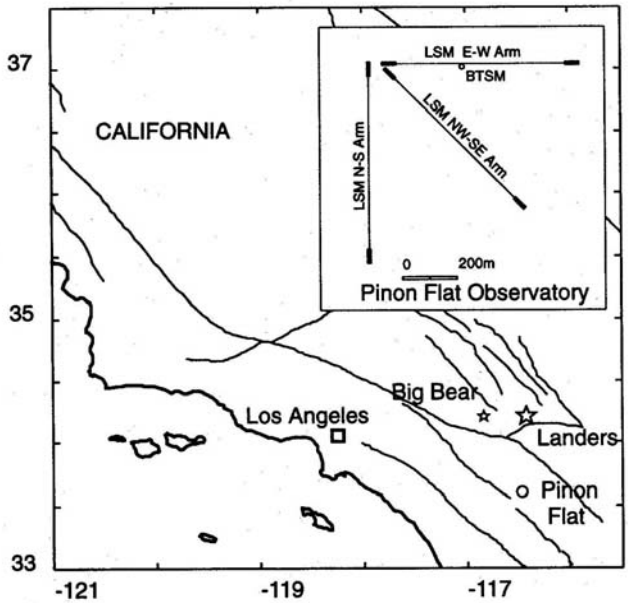

Figure 1. The location of the Pinon Flat Observatory in southern California. The epicenters of the 1992 Landers and Big Bear earthquakes are also shown. The insert shows a plan view of the borehole tensor strain meter (BTSM) and the three arms of the laser strain meter (LSM).

In this paper we establish a matrix representation of the relationship between instrument and remote strains and develop a method for determining this matrix by tidal calibration. We will refer to this method as a cross-coupled calibration. (A matrix description of strain coupling into strain meters was first suggested by *King et al.* [1976], who also proposed a method of calibration using Earth tides.) The calibration method is applied to the Piñon Flat BTSM, using the tides from the colocated laser strain meter (LSM) as the reference signal to eliminate any error in the theoretical tidal estimates. (The LSM measures horizontal deformations in the N-S, E-W, and NW-SE directions over lengths of ~800 m, using interferometry in a vacuum, and so provides average strains over an area of order 1 km^2 [see *Agnew*, 1986].) Figure 1 shows the site location. The calibration is compared with a calibration using theoretical tides to indicate the accuracy to be expected from calibration at other borehole strain meter sites. The potential of the cross-coupling calibration to improve coseismic strain estimates is demonstrated by analysis of the strain offsets of the 1992 Landers earthquake.

Strain Coupling Into Borehole Strain Meters

The 3×1 strain array $\mathbf{s}$ is a convenient description of near surface strains measured by tensor borehole strain meters. Following *Frank* [1966], it is defined in terms of the tensor strain components ε_{ij} (using a 1-east, 2-north axis system) as

$$\mathbf{s}=\begin{bmatrix} e_a \\ \gamma_1 \\ \gamma_2 \end{bmatrix}=\mathbf{A}\begin{bmatrix} \varepsilon_{11} \\ \varepsilon_{22} \\ \varepsilon_{12} \end{bmatrix} \quad \text{where} \quad \mathbf{A}=\begin{bmatrix} 1 & 1 & 0 \\ 1 & -1 & 0 \\ 0 & 0 & 2 \end{bmatrix}. \tag{1}$$

For a vertical borehole, e_a is the areal strain in the plane parallel to the nearby free surface. γ_1 and γ_2 are shear strains whose principal axes are parallel to and 45° to the axis system, respectively. They are both engineering shears. This description has the useful property of separating areal and shear strains which are coupled unequally into borehole strain meters.

The purpose of calibration is to determine the relationship between the remote strains $\mathbf{s}^R$, and the strains $\mathbf{s}^I$ measured by the instrument. As the strains observed are typically small, a linear coupling model

$$\mathbf{s}^I=\mathbf{K}\,\mathbf{s}^R \tag{2}$$

is the most general form, where $\mathbf{K}$ is a 3×3 matrix, the coupling matrix. The diagonal elements of this matrix represent direct coupling, for example, of remote areal strain into instrument areal strain, whereas the off-diagonal terms represent cross coupling. For isotropic coupling as described by *Gladwin and Hart* [1985], the coupling matrix is

$$\mathbf{K}_H=\begin{bmatrix} c & 0 & 0 \\ 0 & d & 0 \\ 0 & 0 & d \end{bmatrix}. \tag{3}$$

No cross coupling is involved.

Cross coupling can be introduced in several ways. One source is the pervasive phenomenon of geological heterogeneity [*Evans et al.*, 1979; *Harrison*, 1985; *Sato and Harrison*, 1990]. When small-scale geological heterogeneity is present, the perturbed strains $\mathbf{s}^P$ in the immediate vicinity of a strain meter can be related to the remote strains $\mathbf{s}^R$ by a 3×3 perturbation matrix **P**, as

$$\mathbf{s}^P = \mathbf{P}\mathbf{s}^R \tag{4}$$

provided the wavelengths of the remote strain field are much larger than the heterogeneity wavelengths [*Berger and Beaumont*, 1976]. Off-diagonal terms in **P** of order 0.2 are not unexpected [*Berger and Beaumont*, 1976; *Sato and Harrison*, 1990]. If the strains just external to the borehole are isotropicly coupled into the instrument (as represented by the diagonal matrix $\mathbf{K}_H$), the coupling matrix between the remote and instrument strain states becomes

$$\mathbf{K} = \mathbf{K}_H\mathbf{P}. \tag{5}$$

Cross coupling in the perturbation matrix thus transfers into the coupling matrix.

The perturbations included in the coupling model need to be selected carefully. Large- and intermediate-scale perturbations are more properly included in source modeling (such as the inhomogeneous modeling of earthquake sources by *Du et al.* [1994]) as they do not meet the above wavelength criterion. The coupling model should rather correct for the small-scale perturbations which are of no interest in tectonic studies, by relating the instrument strains to the average Earth strains over an area typically $1\,\mathrm{km}^2$. The separation of large- and small-scale perturbations is an acceptable working principle analogous to the zooming principle used in finite element modeling [*Desai and Abel*, 1971]. Correcting for small-scale perturbations with the coupling model addresses a significant criticism of short baseline strain measurement, namely, that it is not representative of larger-scale tectonic strains.

Other situations which convert simple coupling to the cross-coupled form, including borehole irregularities, anisotropy, topographic perturbations, and instrument artifacts, are discussed in Appendix A. While some of the effects are minor, particularly the instrumental artifacts and topography perturbations for sites with gentle terrain, other effects can be 10% or more, comparable to the more significant geological perturbations.

In practice it is convenient to determine the remote strain $\mathbf{s}^R$ (defined by (1)) from the instrument readings **e** (radial strains within the instrument) using a calibration equation

$$\mathbf{s}^R = \mathbf{S}\mathbf{e} \tag{6}$$

and relate the calibration matrix **S** to the coupling matrix **K** of (2). For transducers measuring radial strain at selected azimuths, the transducer readings e_j are related to the instrument strains $\mathbf{s}^I$ by [*Jaeger and Cook*, 1979, pp. 39-40]

$$e_j = \tfrac{1}{2}e_a^I + \tfrac{1}{2}\gamma_1^I\cos2\theta_j + \tfrac{1}{2}\gamma_2^I\sin2\theta_j \tag{7}$$

where each transducer azimuth θ_j is measured counterclockwise from the 1 axis. For a set of three transducer readings **e**, (7) may be written in matrix form as

$$\mathbf{e} = \mathbf{O}\mathbf{s}^I \tag{8}$$

where **O** is the transducer orientation matrix defined by

$$\mathbf{O} = \begin{bmatrix} \tfrac{1}{2} & \tfrac{1}{2}\cos2\theta_1 & \tfrac{1}{2}\sin2\theta_1 \\ \tfrac{1}{2} & \tfrac{1}{2}\cos2\theta_2 & \tfrac{1}{2}\sin2\theta_2 \\ \tfrac{1}{2} & \tfrac{1}{2}\cos2\theta_3 & \tfrac{1}{2}\sin2\theta_3 \end{bmatrix}. \tag{9}$$

Using (2) and (8), a transducer coupling equation relating the transducer readings **e** and the remote strains $\mathbf{s}^R$ is

$$\mathbf{e} = \mathbf{C}\,\mathbf{s}^R \tag{10}$$

where the transducer coupling matrix **C** is

$$\mathbf{C} = \mathbf{O}\mathbf{K} \tag{11}$$

The calibration equation (equation (6)) is just the inversion of (10), and the calibration matrix **S** is

$$\mathbf{S} = \mathbf{C}^{-1} = \mathbf{K}^{-1}\mathbf{O}^{-1}. \tag{12}$$

Calibration Method

When cross coupling is included, the nine elements of the calibration matrix **S** must be determined from the calibration equation (equation (6)), using known remote strains $\mathbf{s}^R$ and the corresponding transducer readings **e**. This reduces to independently solving three equations, each containing three parameters. For example, the first equation is

$$e_a^R = s_{11}e_1 + s_{12}e_2 + s_{13}e_3 \tag{13}$$

and the three parameters are s_{1i}. A minimum of three independent measurements of the variables e_a^R, e_1, e_2 and e_3 are required to solve this equation.

The technique used involves the comparison of a known reference signal and the corresponding signal in the strain meter records. The Earth strain tide, the best-known signal in strain meter data, is used here as the reference signal and is obtained from theoretical calculations described later. The observed tidal signal is extracted from the strain meter data records using standard analysis procedures [*Agnew*, 1979; *Ishiguro and Tamura*, 1985], which essentially least squares fit for the amplitudes and phases of sinusoids at the accurately known tidal frequencies. As the procedures effectively narrowband filter the data record at the tidal frequencies [*Hart*, 1996], errors in the determined tides from other signals in the strain records (measurement noise, tectonic events or thermally or groundwater-induced strain disturbances) are largely removed. The raw data records are preprocessed to remove trends, offsets, and any bad data. Interpolation over gaps is not required as missing data are managed automatically by the analysis procedures. For calibration, the largest diurnal and semidiurnal lunar tidal components O_1 (25.82 hours) and M_2 (12.42 hours) are used instead of the complete tidal record, because tidal components with periods near 24 hours and its harmonics may be thermally contaminated. For these components, it was not found necessary to include atmospheric pressure records in the tidal analysis. This is because the strain sensitivity is small (~1 nε/mbar) and most of the power in pressure is at periods of 24 hours and its harmonics. As each tidal component has two parts (represented here by real and imaginary components), a total of four sets of tidal variables are available. Small corrections are applied for phase lags introduced by filters in the instrumentation.

Using the four sets of variables provided by the tidal analysis, each of the three overdetermined equations (like

equation (13)) are solved for the elements of the calibration matrix, using least squares techniques. For example, the equation to relate the remote areal strain to the tides measured by the transducers is

$$\begin{bmatrix} \mathrm{Re}(e_a^{O_1}) \\ \mathrm{Im}(e_a^{O_1}) \\ \mathrm{Re}(e_a^{M_2}) \\ \mathrm{Im}(e_a^{M_2}) \end{bmatrix} = \begin{bmatrix} \mathrm{Re}(e_1^{O_1}) & \mathrm{Re}(e_2^{O_1}) & \mathrm{Re}(e_3^{O_1}) \\ \mathrm{Im}(e_1^{O_1}) & \mathrm{Im}(e_2^{O_1}) & \mathrm{Im}(e_3^{O_1}) \\ \mathrm{Re}(e_1^{M_2}) & \mathrm{Re}(e_2^{M_2}) & \mathrm{Re}(e_3^{M_2}) \\ \mathrm{Im}(e_1^{M_2}) & \mathrm{Im}(e_2^{M_2}) & \mathrm{Im}(e_3^{M_2}) \end{bmatrix} \begin{bmatrix} s_{11} \\ s_{12} \\ s_{13} \end{bmatrix}. \quad (14)$$

Though more sophisticated inversion techniques, such as robust inversions or treatment of errors in all variables, could have been adopted, the simple method was justified by the quality of the inversion residuals. A comparison of the residual of the remote strains to the variations expected from tidal measurement errors indicates the quality of the fit. If the residual is acceptable, we estimate the errors in the calibration matrix elements from the standard deviation σ of the residual, using standard least squares techniques and assuming random measurement errors. This gives the variance of parameter a_i as

$$\sigma_{a_i}^2 = \sigma^2 (\mathbf{M}^{-1})_{ii} \quad (15)$$

where $\mathbf{M}$ is the least squares measurement matrix. If the least squares residual is significantly larger than estimated measurement errors, error in the reference remote strains, inadequacy of the coupling model, or contamination of the strain meter data are indicated.

The errors in a tidal component of angular frequency ω_j are estimated from the variances

$$\sigma_{\mathrm{Re}}^2 = \sigma_{\mathrm{Im}}^2 = \frac{2}{N} P(\omega_j) \quad (16)$$

where $P(\omega_j)$ is the discrete power spectral density of the noise e_r record in the data record (N samples, sampling period t_s), that is,

$$P(\omega) = \frac{1}{N} \left\langle \mathbf{E}(\omega)\mathbf{E}^*(\omega) \right\rangle \text{ where } \mathbf{E}(\omega) = \sum_{r=0}^{N-1} e_r e^{-i\omega r t_s}. \quad (17)$$

The noise power for a specific data record is estimated from the power adjacent to the tidal band of interest, using the power spectrum of the residual from the tidal analysis [*Agnew*, 1979]. This estimate is reliable not only for white noise but for colored noise and transient signals in the data [*Hart*, 1996].

Application of the Calibration Method to Piñon Flat Observations

The calibration techniques are now applied to the Piñon Flat borehole tensor strain meter PFT. First, Earth tides measured by the colocated laser strain meter are used as the calibration reference, because we consider that these give a reliable determination of average local strain tides over ~1 km^2. A second calibration is then made with the current best estimate of the theoretical tides as the reference signal, to assess likely performance of the calibration technique at other sites where only theoretical Earth tides are available.

Calibration With Laser Strain Meter Tides

The LSM provides high-precision measurement of the Earth tides averaged over a 1 km locality at Piñon Flat. These reference tides allow the calibration procedure and the principle of cross coupling to be tested without the added complexity of uncertainty in theoretical tides.

Table 1. Average Pinon Flat BTSM Transducer Tides, With Standard Deviations (SD) and Standard Errors (SE)

	O_1		M_2	
	Amplitude, nε	Phase	Amplitude, nε	Phase
Transducer 1	8.133	7.38	5.293	71.1
SD	0.022	0.54	0.059	2.3
SE	0.010	0.24	0.027	1.0
Transducer 2	5.961	17.17	26.530	-2.674
SD	0.097	0.56	0.078	0.089
SE	0.043	0.25	0.035	0.040
Transducer 3	8.724	-17.36	16.778	5.286
SD	0.048	0.59	0.067	0.084
SE	0.022	0.26	0.030	0.037

For the period 1985 to 1990 inclusive.

The amplitudes and phases of the O_1 and M_2 transducer tides for the Piñon Flat BTSM are given in Table 1. These are averages of yearly determinations over the period 1985 to 1990. The phase convention adopted is that negative phases imply strain lags relative to the local tidal potential, with extensional strain positive. The reproducibility year to year of the tidal determinations is summarized in Table 1 by standard deviations (SD). Standard errors (SE) are given to indicate accuracy of the overall results, assuming no systematic variations are present. For 1 standard error, amplitudes and phases are determined to better than ±0.8% (±0.04 nε) and ±0.3°, apart from transducer 1 M_2.

Figure 2 illustrates with transducer 1 the year to year reproducibility of the determined tides. This is generally in accord with the error bars obtained with (16). The exception is the M_2 phase, which exhibits a systematic drift of about −1°/year, well outside the error estimates. This drift is not apparent on O_1 or on the other transducers, and so is not caused by changes in transducer gain or instrument coupling. It is suggestive of groundwater effects, where resistive and capacitive elements introduce frequency dependent response into tidally induced groundwater flow [*Roeloffs et al.*, 1989]. Small strain amplitude variations of ~0.1 nε/year may then be produced by hydraulic forcing in rock fractures at this site [*Evans and Wyatt*, 1984]. The M_2 phase of transducer 1 is particularly sensitive to remote strain amplitude variations, because the remote areal and shear strain contributions largely cancel each other. This effect is discussed further by *Hart* [1996, pages 4-27 ff.].

Average instrument strain tides for the BTSM for the period 1985 to 1990 are shown in Table 2. These are obtained using the inverse of (8) and the average transducer tides from Table 1, represented as complex numbers. Transducer orientations, counterclockwise from east, are 24.5°, 84.5°, and 144.5° (±2°). For 1 standard error, the areal strains are determined to within ±0.3% and ±0.1°, and shear strains to within ±1.5% and ±0.4°. The standard deviations show that there are no major systematic variations in the strain components. There is no evidence of the M_2 phase drift for transducer 1, confirming the above assertion of high sensitivity of M_2 phase to amplitude variations for the orientation of this transducer.

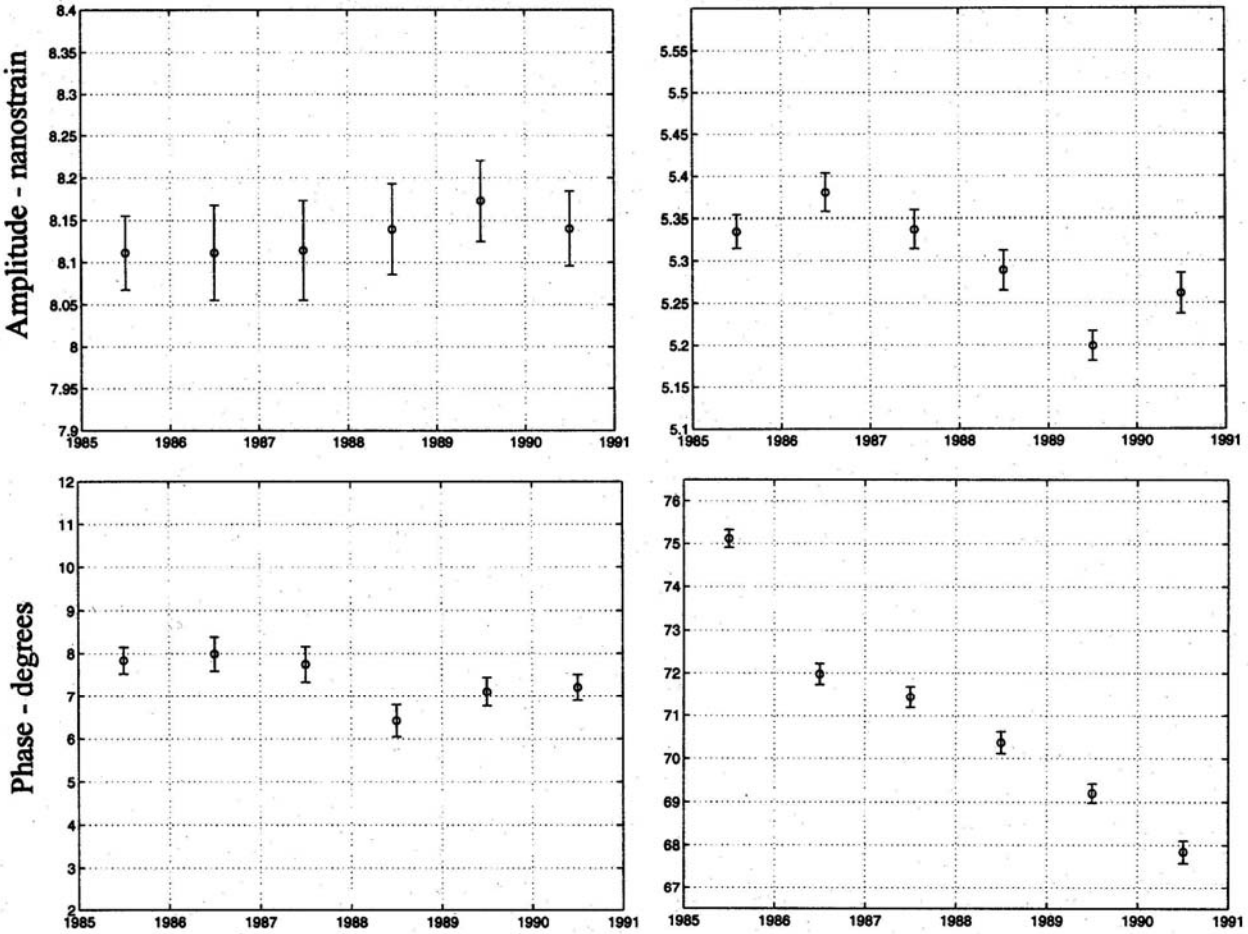

Figure 2. The amplitude and phase for the BTSM transducer 1 (left) O_1 and (right) M_2 tides for each year from 1985 to 1990, with error estimates obtained from the residual power spectral density. Variations in amplitudes and O_1 phase are generally compatible with the estimated errors, but the systematic decrease in M_2 phase of about 1° per year is clearly outside measurement errors. The M_2 phase for this transducer is particularly sensitive to small-amplitude variations in the remote tides, possibly caused by hydrological effects.

The tides for the LSMs are given in Table 3. Analysis details and sample window are the same as for the BTSM. For 1 standard error, the tides are determined to better than ±1.5% (±0.5 nε) for amplitude and ±0.5° for phase. These results agree with a previous determination [*Agnew*, 1979] within the estimated errors, indicating that no significant change in the LSM tides has occurred over a decade. There are some differences from an earlier determination by *Beaumont and Berger* [1975], who used a much shorter span of data.

Table 2. Average BTSM Strain Tides in the Instrument, With Standard Deviations (SD) and Standard Errors (SE)

	O_1		M_2	
	Amplitude, nε	Phase	Amplitude, nε	Phase
e_a	14.730	0.45	30.119	6.785
SD	0.097	0.22	0.122	0.145
SE	0.044	0.10	0.055	0.065
γ_1	4.069	-38.35	26.847	165.543
SD	0.133	0.91	0.308	0.141
SE	0.060	0.41	0.138	0.063
γ_2	4.879	100.86	12.866	167.58
SD	0.159	0.71	0.155	0.49
SE	0.071	0.32	0.069	0.22

Obtained from the transducer tidal components using (8).
For the period 1985 to 1990 inclusive.

The LSM strain tide (determined as for the BTSM, with transducer directions of 0°, –45°, and 90°) are shown in Table 4. For 1 standard error, areal strains are determined to better than ±1% (±0.08 nε) and ±0.2°, and shear strains to better than ±2% (±0.04 nε) and ±2°. The largest errors are for the phases of the O_1 shear tides.

Calibration with isotropic coupling. The method of Appendix B produced the coupling parameters

$$c = 1.73 \pm 0.01$$
$$d = 2.86 \pm 0.16 \quad . \tag{18}$$

The corresponding calibration matrix, from (3) and (12), is

$$\mathbf{S} = \begin{bmatrix} 0.386 & 0.386 & 0.386 \\ 0.306 & -0.458 & 0.152 \\ 0.352 & 0.089 & -0.441 \end{bmatrix} \pm \begin{bmatrix} 0.002 & 0.002 & 0.002 \\ 0.017 & 0.025 & 0.008 \\ 0.020 & 0.005 & 0.025 \end{bmatrix} . \tag{19}$$

The polar plots in Figure 3 compare the strain tides from the LSM (L) and the BTSM (B, obtained from the transducer tides and the above calibration matrix). The areal strains show

Table 3. Average Pinon Flat LSM Tides, With Standard Deviations (SD) and Standard Errors (SE)

	O_1		M_2	
	Amplitude, nε	Phase	Amplitude, nε	Phase
EW LSM	5.134	-9.230	5.358	20.179
SD	0.092	0.495	0.032	0.247
SE	0.041	0.221	0.014	0.111
NW-SE LSM	4.729	-11.454	12.621	0.091
SD	0.038	0.317	0.028	0.197
SE	0.017	0.142	0.012	0.088
NS LSM	3.628	9.03	12.293	-0.906
SD	0.118	1.08	0.065	0.324
SE	0.053	0.48	0.02	0.145

For the period 1985 to 1990 inclusive.

acceptable agreement in amplitude and phase, though differences are well outside the estimated errors. However, for the shears, a value for d some 30% to 45% smaller than 2.86 is required for O_1 γ_1 and M_2 γ_2, but a value larger by 25% for M_2 γ_1. Phase differences are uniformly larger than expected from error estimates. We conclude that isotropic coupling is an inadequate description of strain coupling into the Piñon Flat BTSM. Note also the discrepancy between LSM (L) and theoretical (T) tidal strains in Figure 3. The causes for this are discussed below.

Calibration with cross coupling. The calibration matrix

$$\mathbf{S} = \begin{bmatrix} 0.327 & 0.338 & 0.472 \\ 0.209 & -0.474 & 0.295 \\ 0.441 & -0.032 & -0.469 \end{bmatrix} \pm \begin{bmatrix} 0.016 & 0.013 & 0.021 \\ 0.007 & 0.006 & 0.010 \\ 0.008 & 0.007 & 0.012 \end{bmatrix} \quad (20)$$

was obtained. The comparison of LSM and BTSM strain tides in Figure 4 shows that this calibration has brought the BTSM essentially into agreement with the LSM, within measurement errors. The standard deviations of the residuals are 0.22 nε for areal strain and 0.12 nε for shear strains, close to the expected standard deviations of 0.07 nε and 0.07 nε, respectively. Shear phases have been brought into agreement, and shear amplitudes are consistent for γ_1 and γ_2, for both O_1 and M_2. The coupling matrix is, from (12),

$$\mathbf{K} = \mathbf{O}^{-1}\mathbf{S}^{-1} = \begin{bmatrix} 1.778 & -0.159 & 0.268 \\ -0.032 & 2.689 & 0.731 \\ 0.146 & -0.600 & 2.456 \end{bmatrix}. \quad (21)$$

If the cross coupling is produced by small-scale perturbation of otherwise isotropic coupling across the borehole, the perturbation matrix can be obtained from (5), if the isotropic coupling parameters c and d are known. That is,

$$\mathbf{P} = \mathbf{K}_H^{-1}\mathbf{K} = \begin{bmatrix} 1/c & 0 & 0 \\ 0 & 1/d & 0 \\ 0 & 0 & 1/d \end{bmatrix} \mathbf{K}. \quad (22)$$

Reasonable estimates for the values of c and d, guided by the diagonal elements of $\mathbf{K}$, are 1.8 and 2.6. These are compatible with values from *Gladwin and Hart* [1985] for rock properties at Piñon Flat, and with the isotropic calibration. For these values of c, d, and $\mathbf{K}$, the perturbation matrix of (4) is

$$\mathbf{P} = \begin{bmatrix} 0.988 & -0.088 & 0.149 \\ -0.012 & 1.034 & 0.281 \\ 0.056 & -0.231 & 0.945 \end{bmatrix}. \quad (23)$$

Note that the first row of $\mathbf{P}$ is proportional to $1/c$ while the others are proportional to $1/d$, so that the directly coupled perturbations (the difference of the diagonal terms of $\mathbf{P}$ from 1) are sensitive to the choice of c and d. Cross coupling is represented by the off-diagonal terms. For the chosen values of c and d, the directly coupled perturbations are less than 6% away from 1, whereas some cross-coupled perturbations are up to 28%. These are too large for small-scale topographic effects [*Berger and Beaumont*, 1976] but could be produced by small-scale geological inhomogeneity. *Wyatt* [1989] shows that the effects on seismic velocity of joints in the granodiorite of Piñon Flat have diminished greatly by ~30 m depth. However, a deeper fracture of major dimension (R=80 m), detected at 100 m depth by *Evans and Wyatt* [1984], 50 m above the BTSM, could be responsible for the estimated effects.

Calibrations with simpler coupling models. Other calibrations with the coupling models of Appendix A were also investigated for alternate explanations of the differences between the LSM and BTSM tides. The methods are outlined in Appendix B, and the results are given in Table 5. Though these coupling models reduced the residuals, in no case were the residuals reduced close to the expected residuals based on measurement errors, and the reductions achieved required unlikely parameter values. With more reasonable parameter values, none of the calibrations achieved the match between the two instruments shown in Figure 4. It is possible that some of these effects are present combined with a perturbation, but this cannot be determined from the calibration. We conclude that the cross-coupled coupling model is required for the Piñon Flat BTSM.

Implications of neglecting cross coupling. It is instructive to consider the implications of using the isotropic calibration when cross coupling is present. The difference between the strains s_I determined from transducer observations $\mathbf{e}$ with an isotropic calibration matrix $\mathbf{S}_I$, and the strains s_X determined with a cross-coupled calibration matrix $\mathbf{S}_X$, is

Table 4. Average LSM Strain Tides, With Standard Deviations (SD) and Standard Errors (SE)

	O_1		M_2	
	Amplitude, nε	Phase	Amplitude, nε	Phase
e_a	8.658	-1.65	17.387	5.465
SD	0.181	0.52	0.080	0.196
SE	0.081	0.23	0.036	0.088
γ_1	2.023	-43.3	7.556	164.376
SD	0.066	3.4	0.073	0.589
SE	0.030	1.5	0.033	0.263
γ_2	1.735	109.8	8.087	168.58
SD	0.094	4.0	0.093	0.73
SE	0.042	1.8	0.042	0.33

Obtained from the transducer tidal components using (8).
For the period 1985 to 1990 inclusive.

Table 5. Additional Calibrations of the Pinon Flat BTSM With the LSM as Reference

Effect	Calibration Parameters		e_a Residuals, nε		Shear Residuals, nε	
	Determined	Expected	Determined	Expected	Determined	Expected
None (isotropic)	$c = 1.725 \pm 0.011$ $d = 2.857 \pm 0.158$		0.294	0.067	1.44	0.070
Compass Error	$c = 1.725 \pm 0.011$ $d = 2.676 \pm 0.030$ $\phi = -10.24 \pm 0.33°$	 ±2° max	0.294	0.067	0.315	0.071
Transducer Factors	$c = 1.636 \pm 0.056$ $d = 2.334 \pm 0.097$ $f_2/f_1 = 0.790 \pm 0.030$ $f_3/f_1 = 1.155 \pm 0.044$	 0.9 to 1.1 0.9 to 1.1	0.435	0.067	0.596	0.071
Compass and Factors	$c = 1.837 \pm 0.021$ $d = 2.772 \pm 0.034$ $\phi = -7.76 \pm 0.31°$ $f_2/f_1 = 1.015 \pm 0.014$ $f_3/f_1 = 1.156 \pm 0.014$	 ±2° max 0.9 to 1.1 0.9 to 1.1	0.250	0.066	0.125	0.071

Coupling Models are from Appendix A, and Calibration Methods from Appendix B.
Expected ranges of parameters are from laboratory calibrations and tests with similar transducers.
Standard deviations of the fit residuals are compared to expected residuals based on tidal analysis errors, to assess the validity of the proposed coupling models.

$$\Delta \mathbf{s} = \mathbf{s}_I - \mathbf{s}_X = \mathbf{S}_I \mathbf{e} - \mathbf{S}_X \mathbf{e}$$
$$= \left(\mathbf{S}_I \mathbf{S}_X^{-1} - \mathbf{I}\right)\mathbf{s}_X = \mathbf{E}\mathbf{s}_X \tag{24}$$

where $\mathbf{I}$ is the identity matrix. $\mathbf{E}$ can be seen as the error relative to the calibration represented by $\mathbf{S}_X$. More precisely, the jth element of the ith row of $\mathbf{E}$ represents the fraction of the jth component of the correct remote strains $\mathbf{s}_X$ that appears in error in the ith strain component determined with $\mathbf{S}_I$. For the calibration matrices determined above, the strain errors from using the isotropic calibration with the LSM (obtained from $\mathbf{E}_{I,\mathrm{LSM}} = \mathbf{S}_{I,\mathrm{LSM}}\,\mathbf{S}_{X,\mathrm{LSM}}^{-1} - \mathbf{I}$) are

$$\begin{bmatrix} \Delta e_a \\ \Delta\gamma_1 \\ \Delta\gamma_2 \end{bmatrix} = \mathbf{E}_{I,\mathrm{LSM}} \begin{bmatrix} e_a^R \\ \Delta\gamma_1^R \\ \Delta\gamma_2^R \end{bmatrix}$$
$$= \begin{bmatrix} 0.03 & -0.09 & 0.16 \\ -0.01 & 0.06 & 0.26 \\ 0.05 & -0.21 & -0.14 \end{bmatrix} \begin{bmatrix} e_a^R \\ \Delta\gamma_1^R \\ \Delta\gamma_2^R \end{bmatrix}. \tag{25}$$

Thus, for example, the error in γ_1 estimated with the isotropic calibration is 1% of the remote areal strain, and 6% and 26% of the remote γ_1 and γ_2 shear strains.

Much larger total errors are possible if the strain array components are not comparable in size. This is often the case with strains produced by fault slip, where in the far field of an earthquake, areal and shear coseismic strains exhibit different dependence on azimuth from the epicenter. Dilatational strain measurements are not immune from cross coupling of shear strains. For the Piñon Flat BTSM, 16% of γ_2 shear is cross coupled into areal strain, and unless the shear components are measured there is no direct way of correcting for the error.

Calibration With Theoretical Tides

Since accurately measured local strain tides are not usually available, borehole strain meters are typically calibrated with theoretical tides. Though the tides are the best characterized signal in strain records, the theoretical calculations are not without problems, due to perturbations from poorly known geological inhomogeneity and uncertainties in ocean load tides. The comparison at Piñon Flat of a calibration using theoretical tides with the calibration using the LSM tides therefore provides a useful indication of the accuracy of calibration that might be achieved at other sites.

Calculation of theoretical tides. Three steps are involved in the calculation of Earth strain tides [*Agnew*, 1979; *Harrison*, 1985]. The "body tide" strains for a radially symmetric, oceanless Earth are calculated using solar and lunar ephemerides and Love numbers representing the Earth's elastic response [*Harrison*, 1985]. To these are added the ocean load strain tides calculated from ocean tide maps and surface load Green's functions [*Baker*, 1985] to generate the "homogeneous tide". Last, corrections are applied for perturbations caused by topography and geological inhomogeneity [*Berger and Beaumont*, 1976]. The result is referred to as the "inhomogeneous tide".

The homogeneous tide at Piñon Flat (at 33°36′32.4″ N, 243°32′42″ E, altitude 1280 m) is calculated with the "gotic" program [*Sato and Hanada*, 1984], for the 1066A Earth model and the ocean tide maps of *Schwiderski* [1980]. An estimate $\mathbf{P}_e$ of the Piñon Flat topographic and geological perturbation matrix, derived from *Berger and Beaumont* [1976], is used to calculate the inhomogeneous strain tides $\mathbf{s}_P$ from the homogeneous strain tides $\mathbf{S}_H$,

$$\mathbf{s}_P = \mathbf{P}_e \mathbf{s}_H \tag{26}$$

where

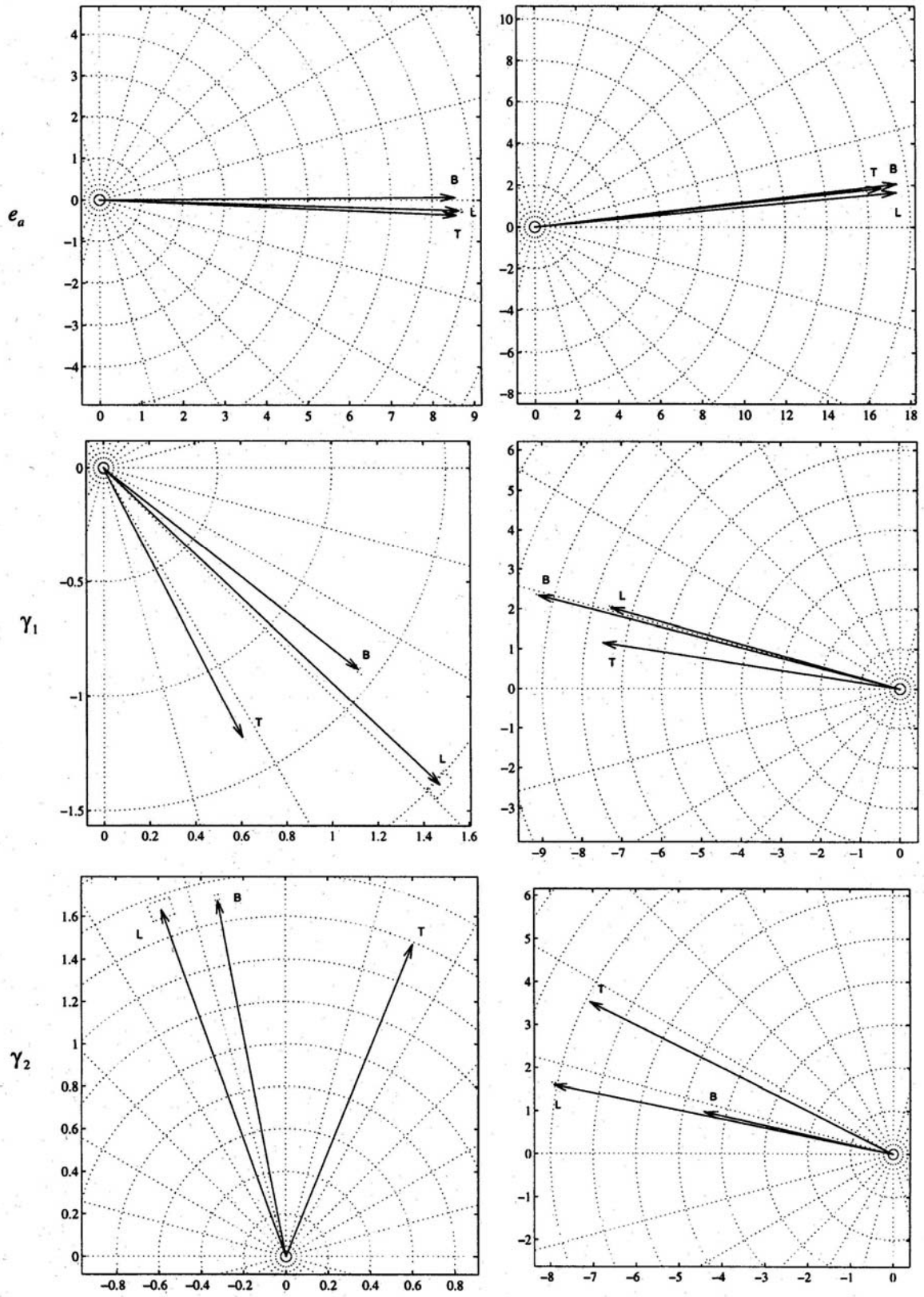

Figure 3. Polar plots of the amplitudes and phases of (left) O_1 and (right) M_2 tidal strains at Pinon Flat. All axes are in nanostrain. The letters indicate B, BTSM with isotropic coupling (c=1.725, d=2.857, from calibration with the LSM); L, LSM; T, theoretical tides. Areal strains show reasonable agreement (though well outside measurement errors), but there are major inconsistencies between the LSM and BTSM shear strains that clearly exceed the measurement errors. Substantial disagreement between the LSM and the theoretical tides is also apparent.

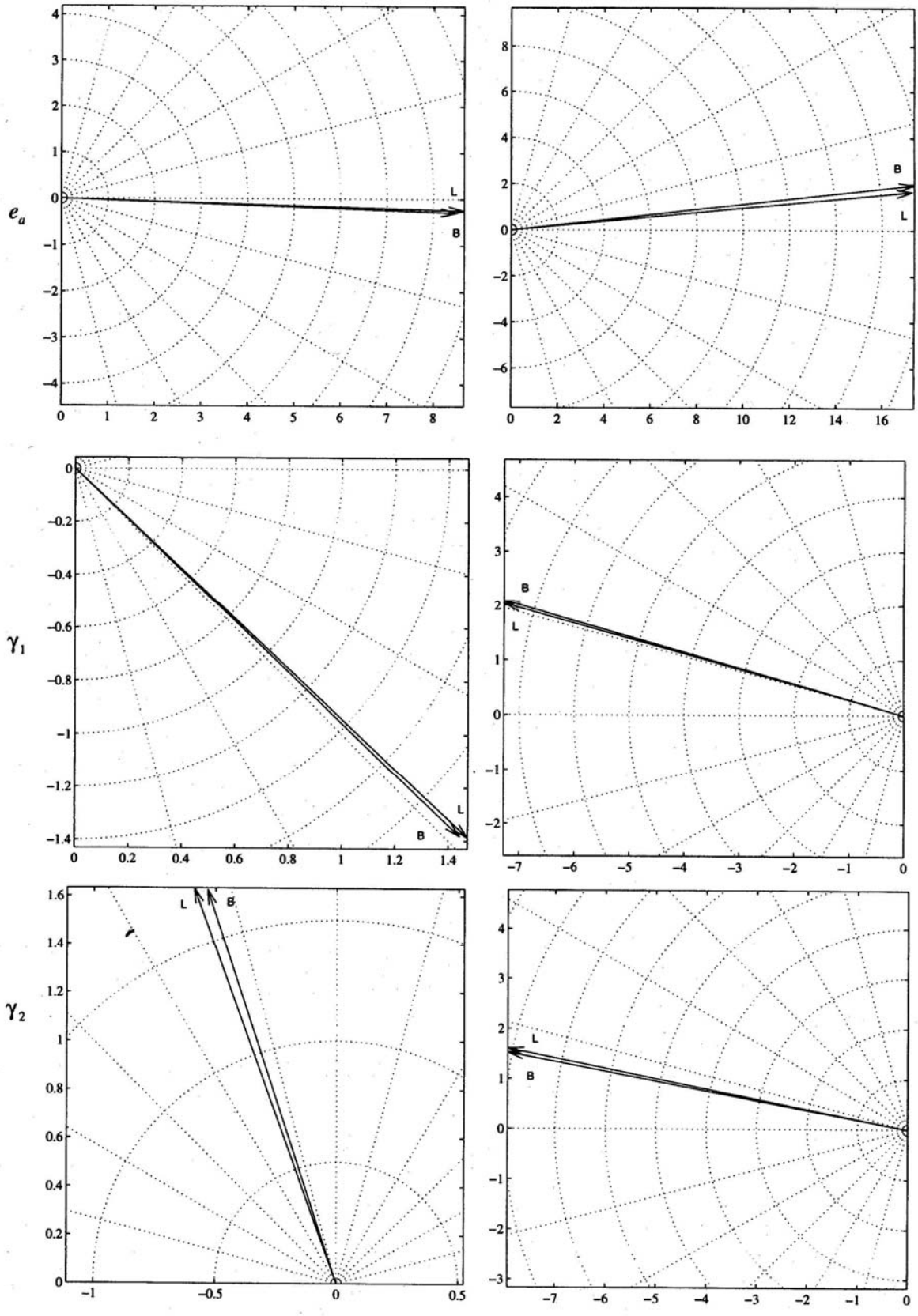

Figure 4. A major improvement in agreement between the BTSM (B) and LSM (L) strain tides is achieved compared to the isotropic calibration of Figure 3, by using the cross-coupled calibration of the BTSM with the LSM as reference. All axes are in nanostrain, (left) O_1 and (right) M_2. The largest improvement is in the shear tides, where both amplitude and phase discrepancies are almost entirely resolved.

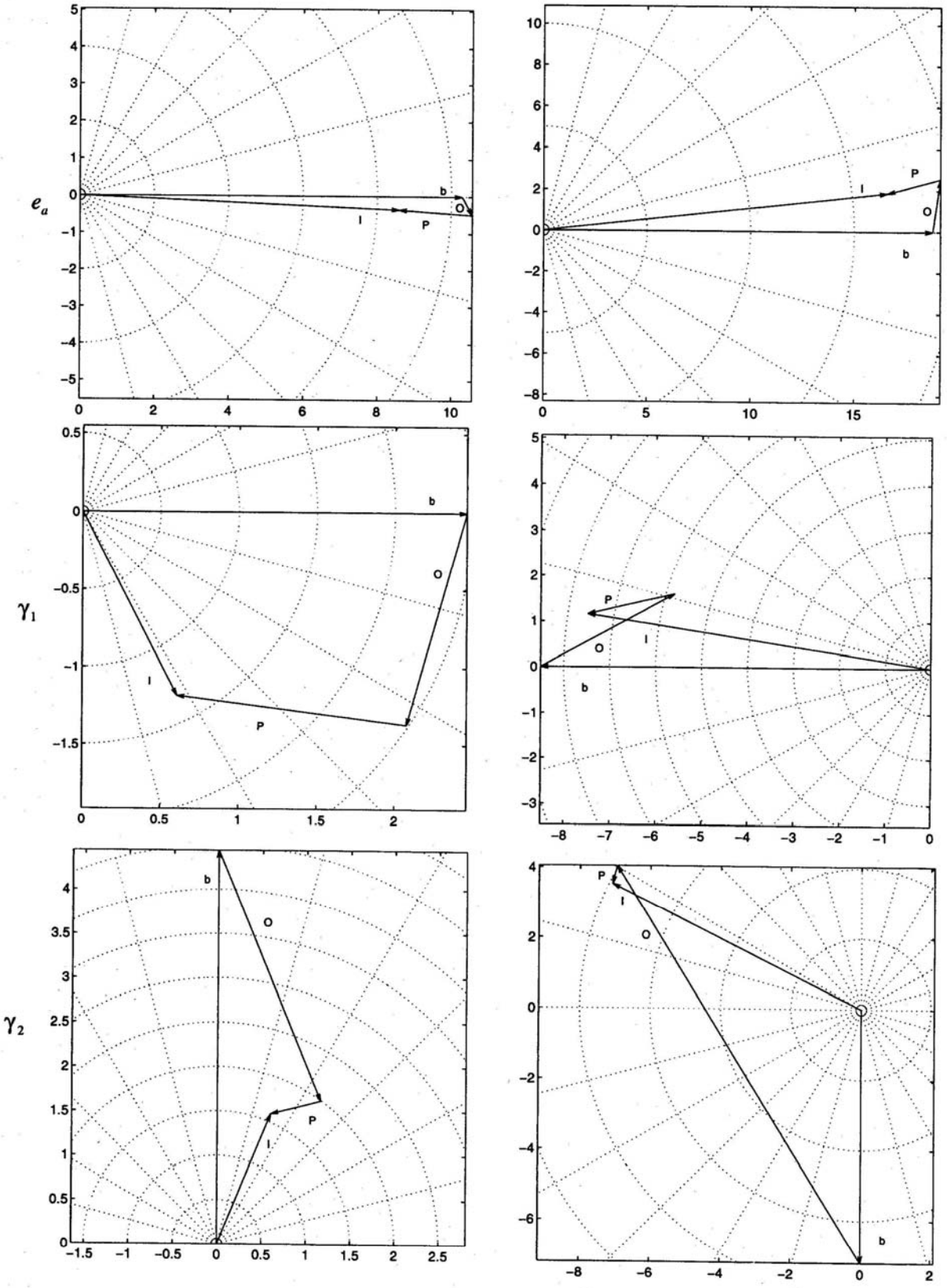

Figure 5. Polar plots of the theoretical inhomogeneous (left) O_1 and (right) M_2 strain tides for Pinon Flat, indicated by (I). All axes are in nanostrain. The contributing parts are the body tide (b), the ocean load tide (O), and the perturbation (P) from topography and geological inhomogeneity.

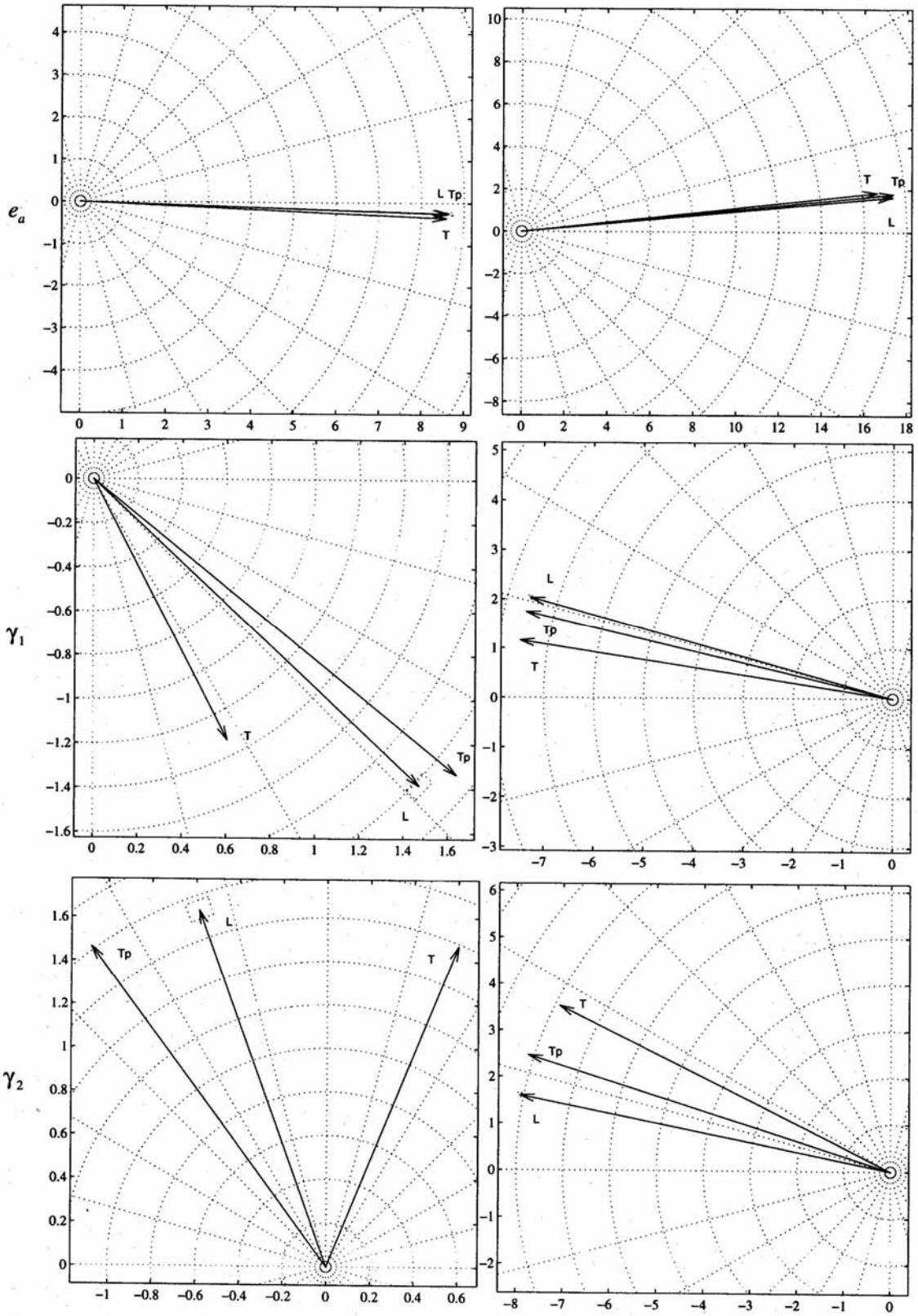

Figure 6. Polar plots comparing LSM (L) and theoretical (Tp and T) O_1 (left) and M_2 (right) strain tides at Pinon Flat. All axes are in nanostrain. The Tp tides are derived from the theoretical homogeneous tide, modified by a perturbation obtained by fitting the homogeneous tide to the LSM observations of the local tide. The T tides include the perturbation determined by *Berger and Beaumont* [1976]. The fitted perturbation improves agreement between theoretical tides and the LSM observations but has not resolved all differences to within LSM measurement errors, particularly the O_1 shear tides.

Table 6a. The Components of the Theoretical Areal Strain Tide at Pinon Flat, for the 1066A Earth Model

	O_1		M_2	
	Amplitude, nε	Phase	Amplitude, nε	Phase
Body	10.292	0.00	18.82	0.00
Ocean Load	0.561	-61.4	2.58	81.7
Homogeneous	10.572	-2.67	19.36	7.58
Inhomogeneous	8.60	-2.4	16.72	6.4

Table 6c. The Components of the Theoretical γ_2 Shear Strain Tide at Pinon Flat, for the 1066A Earth Model

	O_1		M_2	
	Amplitude, nε	Phase	Amplitude, nε	Phase
Body	4.446	90.0	7.206	-90.0
Ocean Load	3.06	-67.6	13.23	121.7
Homogeneous	1.99	54.2	8.05	149.8
Inhomogeneous	1.59	67.8	7.91	153.5

$$\mathbf{P}_e = \begin{bmatrix} 0.832 & -0.074 & -0.035 \\ -0.123 & 0.916 & 0.002 \\ -0.043 & 0.005 & 0.897 \end{bmatrix}. \quad (27)$$

The inhomogeneous strain O_1 and M_2 tides, together with the contributing components (body tide (b), ocean load tide (O), geological and topographic perturbation (P)), are shown in Table 6 and Figure 5.

Within the assumption of radial symmetry, the body tide is probably accurate within a few percent. *Wahr* [1981] showed that the spherical Earth approximation is adequate for 1% accuracy. As an indication of sensitivity to Earth models, calculations were also made with the Gutenberg-Bullen Earth model (GB), which were generally 2-3% higher for areal strain and 1-3% lower for shear strain.

The ocean load tide has a small effect on areal strains (primarily M_2 phase), but a marked effect on shear strains, up to 55% in amplitude (for O_1 γ_1) and 130° in phase (for M_2 γ_2), as seen in Figure 5. The effect of tides in the Gulf of California (>300 km away, ocean tides from *Stock* [1976]) is also significant, up to 60% in amplitude and 25° in phase. Sizeable differences between areal strain load tides for the GB and 1066A Earth models, indicating sensitivity to Green's functions, have only small effects on the homogeneous areal strain tide, because the load tide is comparatively small. For shear tides the differences were 10% or less in amplitude and a few degrees in phase. Given the small amount of continental crust between Piñon Flat and the dominant ocean sources to the west, we prefer the 1066A model over the GB model, which is biased toward continental crust. Some major differences from an earlier result by *Beaumont and Berger* [1975] can be attributed to their use of the less accurate ocean models of that time. We expect there will be some error in our load tides from neglect of the effects of crustal inhomogeneity on the Green's functions. *Mao* [1990] suggests that near-field load tides depend strongly on properties of the crust and upper mantle and that neglect of such effects produces errors larger than errors from cotidal maps. Piñon Flat is 100 km from the ocean and near a continental margin, and so is somewhat sensitive to crustal and upper mantle structure. The modeling of *Beaumont* [1978] showed 10% errors in vertical displacement and 30% in tilt from a continental margin model. Errors of order 10% are to be expected at Piñon Flat.

Table 6b. The Components of the Theoretical γ_1 Shear Strain Tide at Pinon Flat, for the 1066A Earth Model

	O_1		M_2	
	Amplitude, nε	Phase	Amplitude, nε	Phase
Body	2.461	0.0	8.504	180.0
Ocean Load	1.42	-105.7	3.33	28.8
Homogeneous	2.49	-33.4	5.81	164.0
Inhomogeneous	1.33	-62.9	7.57	171.2

The perturbation correction makes substantial changes in some strain tide components. Areal strain is directly reduced by 17% (the $P_{e\,11}$ term) accompanied by 4-7% cross coupling of shear strain. Shear strains are directly reduced by ~10% (the $P_{e\,22}$, $P_{e\,33}$ terms) with minor cross coupling between shears but significant cross coupling (12%) of areal strain into γ_1 (the $P_{e\,21}$ term). As areal strain tides are larger than shears by factors of 2 to 4, the cross coupling can produce amplitude differences of 50% and major phase changes, as seen in Figure 5.

The accuracy of the perturbation is difficult to estimate. Berger and Beaumont estimate the errors in the topography correction are 3%. The geological model accounts for the rigidity contrast of the 2 km-thick sediments in the Coachella Valley 10 km to the east, and produces effects of 7% or less, generally smaller than the topography. However, southern California is a region of major regional geological contrasts in the crust and upper mantle [e.g., *Mooney and Weaver*, 1989; *Hu et al.*, 1994; *Humphreys and Clayton*, 1990; *Humphreys and Dueker*, 1994], and these effects have not yet been modeled. Modeling by *Harrison* [1976], *Berger and Beaumont* [1976], and *Sato and Harrison* [1990] has shown effects as large as 10% to 30%. Anisotropy in crustal rocks is also a likely source of effects of order 10% that have not been included in the perturbation matrix estimate.

Assessing theoretical tides with LSM observations. An indication of the accuracy of the theoretical estimate of the local strain tides at Piñon Flat can be obtained with a comparison to accurately measured tides from the laser strain meters, which reference their measurements to the wavelength of light.

The O_1 and M_2 theoretical tides (for the 1066A Earth model, from Table 6) and the LSM tides (from Table 4) are compared in the polar plot of Figure 6. The theoretical amplitudes are within 6% of the LSM amplitudes, apart from O_1 γ_1 where the error is 35%. Phase differences are within 1° for areal strain, but up to 40° for shear strain. The differences are generally well outside the measurement errors in the LSM tides. Using real and imaginary components, the rms misfits between theory and the LSM are 0.39 nε for areal strain and 0.97 nε for shear strain, well outside the standard deviations or standard errors in Table 4. Figure 3 shows that in many cases the phases of the LSM agree better with the BTSM

simply calibrated with isotropic coupling, than with the theoretical tides.

A possible explanation of the differences between the LSM tides $\mathbf{s}_{LSM}$ and the theoretical tides is error in the perturbation matrix estimate $\mathbf{P}_e$ used to obtain the inhomogeneous tide from the homogeneous tide (equation (28)). The correct matrix $\mathbf{P}_c$ converts the homogeneous tides to the LSM tides, as

$$\mathbf{s}_{LSM} = \mathbf{P}_c \mathbf{s}_H \tag{28}$$

and can be determined by a least squares procedure analogous to the procedure for estimating the calibration matrix (see equation (6)). Using the theoretical homogeneous tides from Table 6 and the LSM tides from Table 4, the determined perturbation matrix is

$$\mathbf{P}_c = \begin{bmatrix} 0.849 & -0.154 & -0.031 \\ -0.058 & 1.057 & 0.049 \\ -0.163 & -0.116 & 0.758 \end{bmatrix}. \tag{29}$$

Comparison with $\mathbf{P}_e$ shows that additive changes in terms of up to ±0.15 are required. The inhomogeneous theoretical tides (Tp), calculated with this perturbation matrix are compared to the LSM observations (L), in Figure 6. Though better agreement has been achieved, remaining differences are significantly larger than the LSM measurement errors. The standard deviations of the areal and shear strain misfits are 0.12 nε and 0.45 nε, above expected values of 0.07 nε based on LSM errors. A comparison with initial misfit standard deviations indicates that only one third to one half of the misfit is accounted for by unmodeled perturbations.

A frequency dependent source of error is therefore indicated, with errors roughly 5% to 10% for areal strain and 15% to 30% for shear strain. The most likely source is the ocean load tide estimates. We are fairly confident in the ocean tide data, so that the Green's functions are suspect. Frequency dependence could be introduced because the frequency dependent ocean tide distributions sample different spatial domains of the Green's functions. The errors have not been identified in earlier studies, because these concentrated on axial strain in transducer directions [*Berger and Beaumont*, 1976; *Sato and Harrison*, 1990], which is dominated by the areal strain component that is less sensitive than shear to load tide errors.

We conclude that current best theoretical estimates of local strain tides are inaccurate at the 0.4 nε level for areal strain and the 1 nε level for shear strain. The percentage errors are therefore significantly larger for shear strain compared with areal strain, because of the differences in areal and shear strain tidal amplitudes.

BTSM calibration with theoretical tides. A BTSM calibration using theoretical tides demonstrates the effects of these errors on the accuracy of calibration.

Calibration with isotropic coupling: Using the isotropic coupling model, the calibration with theoretical tides gave

$$c = 1.79 \pm 0.01$$
$$d = 2.96 \pm 0.18 \quad . \tag{30}$$

These parameters are both about 3% larger than those determined using the LSM tides. This level of agreement reflects the broad agreement between LSM and theoretical tidal amplitudes noted earlier. The residual standard deviations are 0.30 nε for areal strain and 1.53 nε for shear strain, significantly larger than expected standard deviations of 0.03 nε and 0.02 nε.

Calibration with cross coupling: The calibration matrix S for the calibration with cross coupling is

$$\begin{bmatrix} 0.335 & 0.300 & 0.486 \\ 0.119 & -0.433 & 0.230 \\ 0.620 & -0.053 & -0.416 \end{bmatrix} \pm \begin{bmatrix} 0.009 & 0.008 & 0.012 \\ 0.013 & 0.0127 & 0.019 \\ 0.041 & 0.036 & 0.058 \end{bmatrix}. \tag{31}$$

The corresponding coupling matrix **K** is

$$\begin{bmatrix} 1.726 & -0.368 & 0.212 \\ 0.123 & 3.015 & 0.767 \\ -0.353 & -1.079 & 2.022 \end{bmatrix} \tag{32}$$

and shows some major differences in the cross-coupling terms (up to +0.15, -0.5) from the coupling matrix determined with the LSM tides. Such differences are expected given the major phase differences identified in Figure 6. The BTSM tides obtained with this calibration are compared to the theoretical tides and LSM tides in Figure 7. The BTSM tides (B) are closer to the theoretical tides (T) than for the isotropic calibration (see Figure 3), but in several cases have been moved away from the correct LSM tides (L). The residual standard deviations of 0.13 nε and 0.45 nε are reduced by 37% and 70% from the isotropic calibration but are significantly larger than the standard deviations of 0.03 nε expected from BTSM measurement errors. We conclude on the basis of this calibration that there are errors in the theoretical tides, with RMS values at least 0.1 nε for areal strain and 0.4 nε for shear strain. The comparison of theoretical and LSM tides showed RMS errors of 0.4 nε and 1 nε. The cross-coupled calibration matrix has absorbed some of the error in the theoretical tides, producing major errors in the calibration.

The strain errors from using the calibrations made with theoretical tides, expressed in terms of the error matrix of (26), are

$$\begin{bmatrix} \Delta e_a \\ \Delta\gamma_1 \\ \Delta\gamma_2 \end{bmatrix} = \mathbf{E}_{I,T} \begin{bmatrix} e_a{}^R \\ \Delta\gamma_1{}^R \\ \Delta\gamma_2{}^R \end{bmatrix} = \begin{bmatrix} 0.0 & -0.09 & 0.15 \\ -0.01 & -0.09 & 0.25 \\ 0.05 & -0.20 & -0.17 \end{bmatrix} \begin{bmatrix} e_a{}^R \\ \Delta\gamma_1{}^R \\ \Delta\gamma_2{}^R \end{bmatrix} \tag{33}$$

for the isotropic calibration, and

$$\begin{bmatrix} \Delta e_a \\ \Delta\gamma_1 \\ \Delta\gamma_2 \end{bmatrix} = \mathbf{E}_{X,T} \begin{bmatrix} e_a{}^R \\ \Delta\gamma_1{}^R \\ \Delta\gamma_2{}^R \end{bmatrix} = \begin{bmatrix} -0.02 & 0.07 & 0.0 \\ -0.10 & -0.15 & -0.06 \\ 0.19 & 0.17 & 0.18 \end{bmatrix} \begin{bmatrix} e_a{}^R \\ \Delta\gamma_1{}^R \\ \Delta\gamma_2{}^R \end{bmatrix} \tag{34}$$

for the cross coupled calibration. The isotropic calibration errors are comparable to those for the isotropic calibration with the LSM (equation (27)), reflecting the closeness of theoretical and LSM tidal amplitudes. The cross coupling calibration errors are generally not significantly better, being reduced in some cases but increased in others (for example, coupling of areal strain into γ_2).

Discussion

Incorporation of cross coupling into the calibration of the Piñon Flat BTSM significantly improves the accuracy of measurements of tectonic signals. The M7.3 Landers

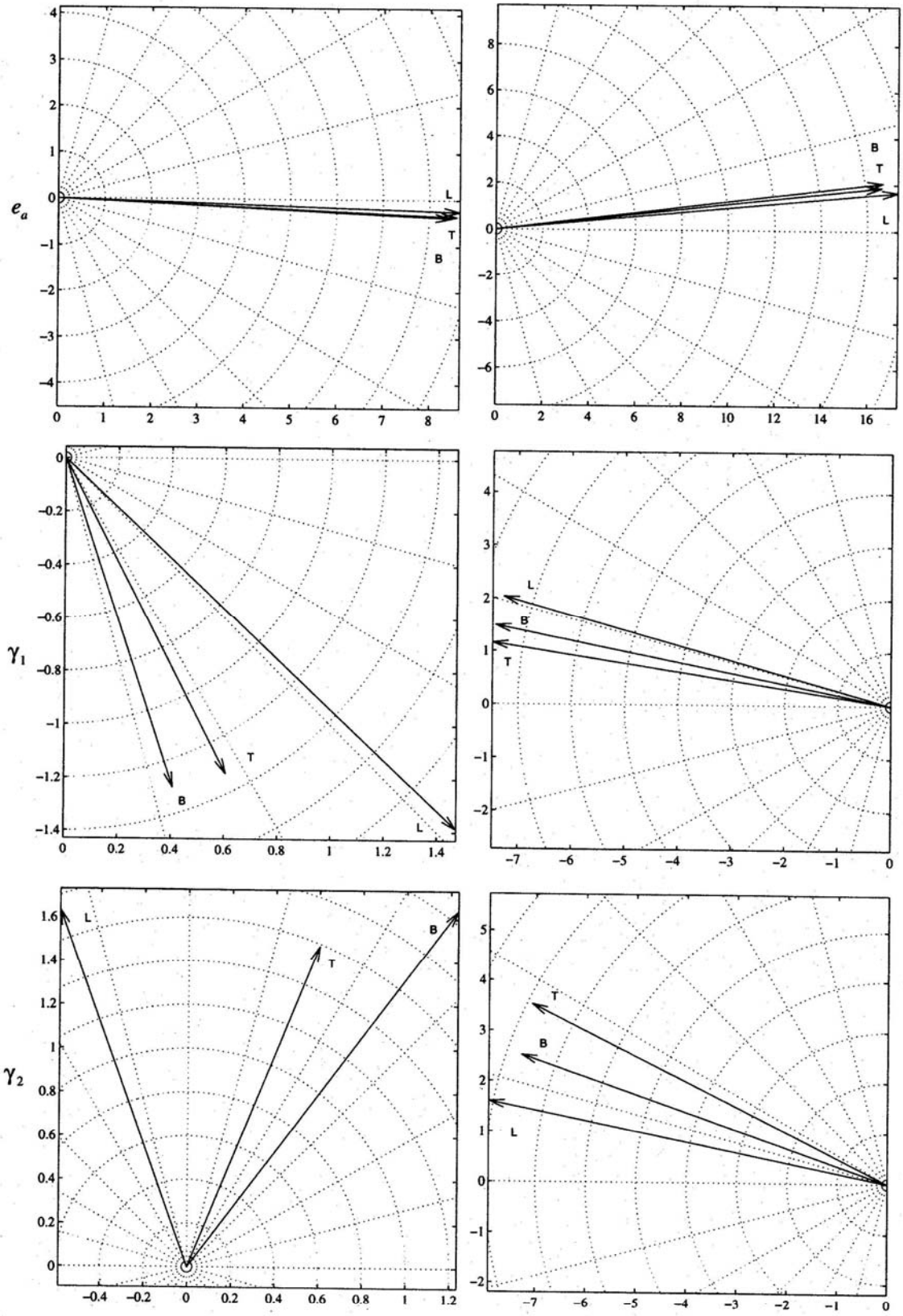

Figure 7. Polar plots for (left) O_1 and (right) M_2 strain tides, comparing the BTSM (B) (using a cross-coupled calibration with theoretical tides), LSM (L), and theoretical tides (T). All axes are in nanostrain. The cross-coupled calibration has achieved a closer fit of the BTSM tides to the theoretical tides than isotropic coupling allowed (see Figure 3). However, in several cases, this has resulted in a greater discrepancy between the BTSM tides and the actual local tides as measured by the LSM. The errors in the theoretical tides, shown in Figure 5, are responsible.

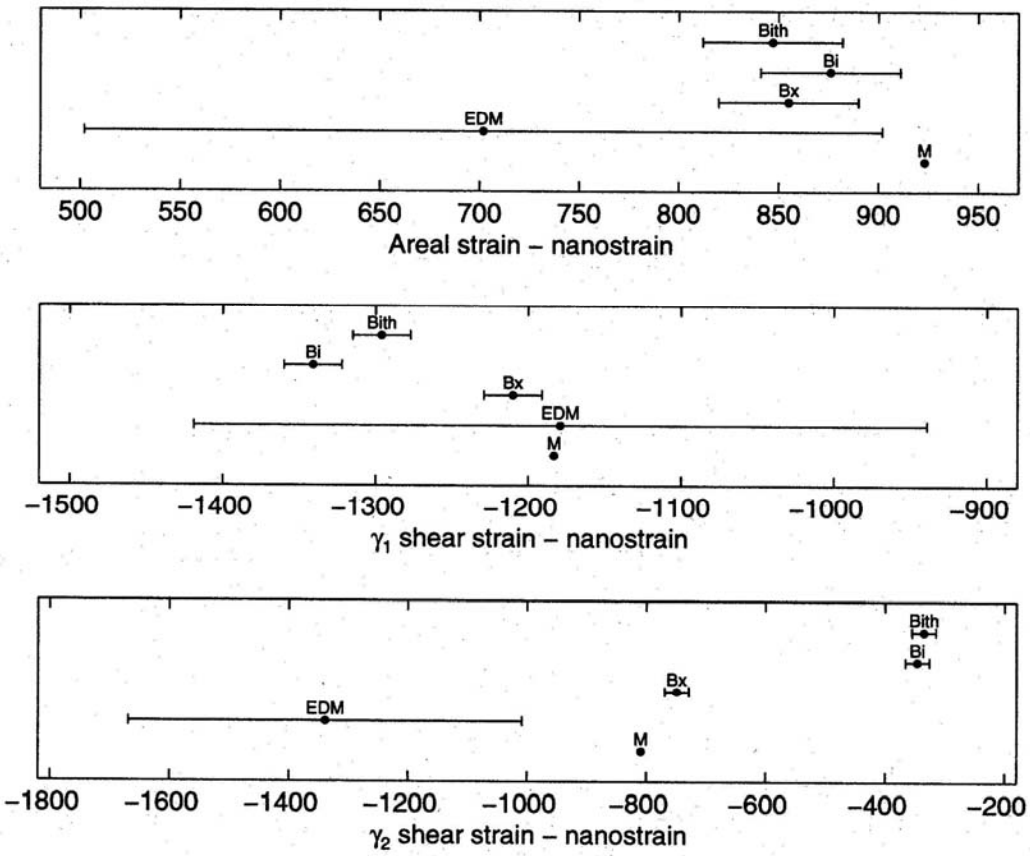

Figure 8. A comparison of strain offsets at Pinon Flat from the combined Landers and Big Bear earthquakes of 1992. The modeled offsets (M) are calculated from the fault model of *Hudnut et al.*, [1994], and the geodetic offsets (EDM) are network-averaged strains for a small network operated by J. Langbein. The BTSM offsets are obtained with the cross-coupled (Bx) and isotropic (Bi) calibrations, both using the LSM as reference, and the isotropic calibration with the theoretical reference (Bith). Significant improvement in agreement between the BTSM and the model shear strain offsets is achieved with the cross-coupled calibration.

earthquake of 1992, some 100 km to the north of Piñon Flat, provided a good example. The BTSM strain offsets for this event were well determined, and reasonable dislocation modeling predictions of these offsets can be made using the well-constrained source models from geodetic inversions [*Hudnut et al.*, 1994]. No other direct strain measurements of the event were available for Piñon Flat [*Wyatt et al.*, 1994; A. T. Linde, personal communication, 1995], but network-averaged strain offsets can be calculated from displacements measured by a nearby two-color electronic distance measurement (EDM) network. Figure 8 compares model predictions, EDM strains, and BTSM strains, for the combined Landers earthquake and the Big Bear aftershock 3 hours later. The EDM strains were obtained by least squares fitting to line-averaged strains, calculated by dividing the displacement offsets in Hudnut's Table 3 by the lengths of the corresponding geodetic lines. Errors are formal fit errors. The BTSM offsets obtained with the cross coupling calibration (Bx) with the LSM are all within 7% of the model offsets (M), whereas the γ_2 offset for the isotropic calibration (Bi) is in error by 57%. Similar errors are found when the isotropic calibration referenced to theoretical tides is used (Bith). The difference arises from 21% cross coupling of the large γ_1 offset into γ_2. The EDM γ_2 offset is clearly not compatible with the BTSM offset for the isotropic calibrations, but, within errors, is compatible with the cross coupled calibration.

The cross coupling calibration of the BTSM overcomes the criticism that short baseline strain meter measurements are unrepresentative of the strain field in a locality. Representative tectonic strains can now be obtained, provided the reference tides used in the cross coupled calibration are accurate (here the LSM tides, but ideally more accurate theoretical tides). The accuracy obtained for both tidal and tectonic strain measurements from the BTSM indicates that, for periods less than a day, the effective BTSM baseline has been extended to that of the LSM, namely, 1 km. With a cross coupled calibration, the baseline of borehole strain is determined by the spatial scale of the calibration reference.

We expect cross coupling to be relevant at the other borehole strain meter sites, since the geological inhomogeneity at Piñon Flat is not exceptional. Neither are other borehole strain meter designs, such as the Sacks-Evertson dilatometer, exempt from cross coupling effects. For the Piñon Flat BTSM, 16% of γ_2 is coupled into areal strain, as shown by (27). In the case of the Landers earthquake, opposing effects of γ_1 and γ_2 fortuitously cancel to produce the small correction for e_a apparent in Figure 8. Generally,

this is not to be expected. For an earthquake producing γ_2 3 times larger than areal strain at Piñon Flat, neglect of cross coupling will produce a 50% error in the determined areal strain. In practice, refinement of the accuracy of dilatometer data requires independent estimates of the shear strains. See Appendix C.

Though cross coupling has been identified at Piñon Flat, it was not possible to determine a cross coupled calibration with theoretical tides, because of demonstrated errors in the ocean load tides and the perturbation estimates. In fact, the accuracy of the cross coupled calibration was little better than the isotropic calibration. The same difficulties may be expected at other sites. The improvement in accuracy and consequent increased utility of borehole strain meter sites makes determination of the cross coupled calibration desirable.

Improvements in the accuracy of theoretical tides are therefore required. Uncertainty about the deep ocean tide contribution to the ocean load tide will be reduced with results from the TOPEX/POSEIDEN project. Improving knowledge of Californian crustal and upper mantle structure [*Mooney*, 1989] can be applied to calculating perturbed ocean load Green's functions and regional geological perturbations. Work is underway on improved finite element modeling, involving digital topography data, finer grids, and more detailed geology. Effects of mantle anelasticity and anisotropy may be included at a later stage, although the review by *Scherneck* [1991] suggests these effects may be below a few percent, particularly for diurnal and semidiurnal tides. The improvements will be evaluated at Piñon Flat before being applied at other sites. Finally, this study reaffirms the crucial role that high-quality reference instruments and observatory-based instrument comparisons play in instrument development and evaluation.

Conclusions

A calibration method that incorporates cross coupling of remote areal/shear strains into instrument shear/areal strains has brought strain tides measured by the Piñon Flat borehole tensor strain meter (borehole diameter 200 mm) into very good agreement with strain tides measured by the colocated laser strain meter (dimensions ~1 km). The cross coupled calibration has also yielded good agreement between the BTSM observations of the 1992 Landers earthquake and geodesy-based modeling and colocated EDM measurements. By extending the small baseline of borehole strain to the spatial scale of the calibration reference, the cross-coupled calibration allows more representative determination of tectonic strain from borehole strain measurements.

Cross coupling needs to be incorporated into calibrations of all short-baseline strain meters, otherwise errors in determined strains of greater than 50% can result, depending on the comparative size of the areal and shear strains. Dilatational strain is not immune to these effects, as shown at Piñon Flat where 16% cross coupling of γ_2 shear into areal strain was determined. Furthermore, corrections cannot be made unless shear strain is measured. Current theoretical strain tide estimates are not accurate enough to determine the cross-coupled calibration, with the largest resultant problems in shear strain measurement. Improvements in the areas of deep ocean tides, inhomogeneous ocean load Green's functions, and topography and geology perturbations, need to be pursued.

Appendix A: Sources of Cross Coupling

Cross coupling of strain into borehole strain meters is introduced by geological inhomogeneity as discussed above and by topography with a similar mechanism. It is also produced by the following conditions.

Orientation Error

For an error $\delta\phi$ in the instrument orientation, so that the correct transducer azimuths θ_j are related to the apparent azimuths θ_j^* by

$$\theta_j = \theta_j^R - \delta\phi \tag{A1}$$

the correct and apparent orientation matrices are related by

$$\mathbf{O} = \mathbf{O}^* \mathbf{R} \quad \text{with} = \begin{bmatrix} 1 & 0 & 0 \\ 0 & \cos 2\delta\phi & -\sin 2\delta\phi \\ 0 & \sin 2\delta\phi & \cos 2\delta\phi \end{bmatrix}. \tag{A2}$$

The apparent instrument strain state $\mathbf{s}^{I*}$ (obtained with the incorrect azimuths) is, from (7), (8) and (9),

$$\mathbf{s}^{I*} = \left(\mathbf{O}^*\right)^{-1}\mathbf{e} = \left(\mathbf{O}^*\right)^{-1}\mathbf{O}\mathbf{K}\mathbf{s}^R = \mathbf{R}\mathbf{K}\mathbf{s}^R. \tag{A3}$$

The apparent coupling matrix is therefore

$$\mathbf{K}^* = \mathbf{R}\mathbf{K}. \tag{A4}$$

If the borehole coupling is isotropic (equation (3)), the apparent coupling matrix has the distinct form

$$\mathbf{K}^* = \begin{bmatrix} c & 0 & 0 \\ 0 & d\cos 2\delta\phi & -d\sin 2\delta\phi \\ 0 & d\sin 2\delta\phi & d\cos 2\delta\phi \end{bmatrix} \tag{A5}$$

with equal second and third diagonal terms (which are close to d for small $\delta\phi$), and two off-diagonal terms which are equal in size and opposite in sign. If the error is not corrected, the coupling has been converted from isotropic coupling to cross coupling, with equal and opposite cross coupling between the shear strain state components. Areal strain and maximum shear strain are unaffected, but the apparent orientation of the principal axes in the instrument, which are parallel to the remote principal axes for isotropic coupling, are rotated $\delta\phi$. The calibration involves three parameters.

Transducer Factors

Transducer factors relate the transducer readings $\mathbf{r}$ to the instrument strains in the transducer directions, as

$$\mathbf{e} = \mathbf{F}\mathbf{r} \text{ with } \mathbf{F} = \begin{bmatrix} f_1 & 0 & 0 \\ 0 & f_2 & 0 \\ 0 & 0 & f_3 \end{bmatrix}. \tag{A6}$$

The factors are close to unity in the BTSM but are not known exactly for earlier instruments. The transducer readings are related to the remote strains, using (9) and (10), by

$$\mathbf{r} = \mathbf{F}^{-1}\mathbf{e} = \mathbf{F}^{-1}\mathbf{O}\mathbf{K}\mathbf{s}^R. \tag{A7}$$

The apparent instrument strain state $\mathbf{s}^{I*}$ calculated from the readings while ignoring the factors is

$$\mathbf{s}^{I*} = \mathbf{O}^{-1}\mathbf{r} = \mathbf{O}^{-1}\mathbf{F}^{-1}\mathbf{O}\mathbf{K}\mathbf{s}^R \tag{A8}$$

and the apparent coupling matrix is

$$\mathbf{K}^* = \mathbf{O}^{-1}\mathbf{F}^{-1}\mathbf{O}\mathbf{K}. \tag{A9}$$

Even if the borehole coupling is isotropic, the apparent coupling matrix will now be non-diagonal unless the factors are equal, and cross coupling will occur between all strain state components. The calibration involves four determinable parameters.

Variations in Coupling Along the Borehole

The BTSM transducers are spaced 160 mm apart along the instrument axis. Variations in rock or grout properties, or borehole irregularities, along the instrument axis will result in different coupling parameters c_j and d_j for each transducer. The transducer coupling matrix is then

$$\mathbf{C} = 1/2\begin{bmatrix} c_1 & d_1\cos 2\theta_1 & d_1\sin 2\theta_1 \\ c_2 & d_2\cos 2\theta_2 & d_2\sin 2\theta_2 \\ c_3 & d_3\cos 2\theta_3 & d_3\sin 2\theta_3 \end{bmatrix} \tag{A10}$$

and the coupling matrix $\mathbf{K} = \mathbf{O}^{-1}\mathbf{C}$ (via equation (10)) is clearly nondiagonal. The coupling is specified by six parameters.

Anisotropy

For anisotropic rock surrounding a borehole, the coupling matrix **C** can be inferred from the analysis by *Amadei* [1983] of deformation of a circular hole in anisotropic rock. By analogy with his equation 43 of Appendix 4.5,

$$\mathbf{C} = 1/2\begin{bmatrix} c_1 & d_{11}\cos 2\theta_1 & d_{12}\sin 2\theta_1 \\ c_2 & d_{21}\cos 2\theta_2 & d_{22}\sin 2\theta_2 \\ c_3 & d_{31}\cos 2\theta_3 & d_{32}\sin 2\theta_3 \end{bmatrix}. \tag{A11}$$

As for the previous case the coupling matrix **K** is nondiagonal and cross coupling results. The parameters c_i and d_{ij} are complicated functions of the elastic parameters. The comparison by *Monaghan* [1990] of strains in isotropic and anisotropic bodies under identical applied stresses suggests that the cross-coupled terms will be of order the fractional differences in elastic parameters from mean parameters. Most rocks are at least moderately anisotropic [*Jaeger and Cook,* 1976, p. 137), with typically 20% variation in elastic parameters. The widespread occurrence of aligned cracks in crustal rocks [*Crampin*, 1987; *Leary et al.*, 1990] is a further source of anisotropy. Therefore cross-coupling effects of order 10% are expected from anisotropy. Nine parameters are required to specify the coupling, equivalent to the general form of coupling of (6).

Appendix B: Additional Calibration Methods

Several forms of borehole strain meter coupling involve fewer parameters than the nine required for general cross coupling. This allows a simpler form of calibration. As for the calibrations described in the Calibration Method section, the real and imaginary components of the O_1 and M_2 tides are used in a least squares procedure. In the following equations, vertical dots mean repeat the above terms for each (real or imaginary) component of each tide.

Isotropic Coupling

Rearrangement of (2) and (3) gives

$$\begin{bmatrix} e_a^R \\ \vdots \end{bmatrix} = \begin{bmatrix} e_a^I \\ \vdots \end{bmatrix}[1/c]$$

$$\begin{bmatrix} \gamma_1^R \\ \gamma_2^R \\ \vdots \end{bmatrix} = \begin{bmatrix} \gamma_1^I \\ \gamma_2^I \\ \vdots \end{bmatrix}[1/d] \quad . \tag{B1}$$

Orientation Error

Rearrangement of the coupling equation (A3) gives two equations

$$\begin{bmatrix} e_a^R \\ \vdots \end{bmatrix} = \begin{bmatrix} e_a^{I*} \\ \vdots \end{bmatrix}[1/c]$$

$$\begin{bmatrix} \gamma_1^R \\ \gamma_2^R \\ \vdots \end{bmatrix} = \begin{bmatrix} \gamma_1^{I*} & \gamma_2^{I*} \\ \gamma_2^{I*} & -\gamma_1^{I*} \\ \vdots & \vdots \end{bmatrix}\begin{bmatrix} p_1 \\ p_2 \end{bmatrix} \text{ with } \begin{matrix} p_1 = (1/d)\cos 2\delta\phi \\ p_2 = (1/d)\sin 2\delta\phi \end{matrix} . \tag{B2}$$

These are solved separately for the parameters $1/c$, p_1, and p_2. The parameters d and $\delta\phi$ are then obtained from

$$1/d = \sqrt{p_1^2 + p_2^2}$$

$$\tan 2\delta\phi = p_2 / p_1 \quad . \tag{B3}$$

Transducer Factors

Rearranging (A7), after dividing through by f_1, gives

$$\begin{bmatrix} r_1 \\ 0 \\ 0 \\ \vdots \end{bmatrix} = \begin{bmatrix} e_a^R & e_\gamma^R(\theta_1) & 0 & 0 \\ e_a^R & e_\gamma^R(\theta_2) & -r_2 & 0 \\ e_a^R & e_\gamma^R(\theta_3) & 0 & -r_3 \\ \vdots & \vdots & \vdots & \vdots \end{bmatrix}\begin{bmatrix} c/f_1 \\ d/f_1 \\ f_2/f_1 \\ f_3/f_1 \end{bmatrix} \tag{B4}$$

where

$$e_\gamma^R(\theta) = \gamma_1^R\cos 2\theta + \gamma_2^R\sin 2\theta \quad . \tag{B5}$$

This can be solved for the four required parameters.

Variations in Coupling Along the Borehole

For each transducer an equation of the form

$$\begin{bmatrix} e_j \\ \vdots \end{bmatrix} = \begin{bmatrix} e_a^R & e_\gamma^R(\theta_j) \\ \vdots & \vdots \end{bmatrix}\begin{bmatrix} c_j \\ d_j \end{bmatrix} \tag{B6}$$

is solved for the transducer specific coupling parameters c_j and d_j.

Compass Error and Transducer Factors

The transducer coupling equation for compass error is, from (A3),

$$\mathbf{e} = \mathbf{O}^*\mathbf{R}\mathbf{K}\mathbf{s}^R . \tag{B7}$$

Rewriting in terms of transducer readings gives, from (A6),

$$\left(\mathbf{O}^*\right)^{-1}\mathbf{F}\mathbf{r} = \mathbf{R}\mathbf{K}\mathbf{s}^R . \tag{B8}$$

Dividing through by f_1 and collecting terms for the parameters to be determined gives

$$\begin{bmatrix} -(O^{-1})_{11} r_1 \\ -(O^{-1})_{21} r_1 \\ -(O^{-1})_{31} r_1 \\ \vdots \end{bmatrix} =$$

$$\begin{bmatrix} -e_a^R & 0 & 0 & (O^{-1})_{12} r_2 & (O^{-1})_{13} r_3 \\ 0 & -\gamma_1^R & \gamma_2^R & (O^{-1})_{22} r_2 & (O^{-1})_{23} r_3 \\ 0 & \gamma_2^R & -\gamma_1^R & (O^{-1})_{22} r_2 & (O^{-1})_{33} r_3 \\ \vdots & \vdots & \vdots & \vdots & \vdots \end{bmatrix} \begin{bmatrix} c/f_1 \\ (d/f_1)\cos 2\delta\phi \\ (d/f_1)\sin 2\delta\phi \\ f_2/f_1 \\ f_3/f_1 \end{bmatrix} \quad \text{(B9)}$$

where the asterisk has been dropped from the **O** matrix terms for clarity. The five parameters are determined concurrently, and the parameters d/f_1 and $\delta\phi$ are recovered as in (B3).

Appendix C: Cross Coupling Correction of Dilatometers

A cross-coupled calibration for the dilatometer is obtained using the first row of the coupling equation (2), namely,

$$e_a{}^I = \begin{bmatrix} K_{11} & K_{12} & K_{13} \end{bmatrix} \begin{bmatrix} e_a{}^R \\ \gamma_1{}^R \\ \gamma_2{}^R \end{bmatrix}. \quad \text{(C1)}$$

The three required elements of the coupling matrix are determined by least squares fitting of observed areal strain tides and reference areal and shear strain tides as

$$\begin{bmatrix} e_a{}^I \\ \vdots \end{bmatrix} = \begin{bmatrix} e_a{}^R & \gamma_1{}^R & \gamma_2{}^R \\ \vdots & \vdots & \vdots \end{bmatrix} \begin{bmatrix} K_{11} \\ K_{12} \\ K_{13} \end{bmatrix}. \quad \text{(C2)}$$

Using this calibration, regional areal strain is recovered from the areal strain measured with the dilatometer by a rearrangement of equation (C1), incorporating estimates of the regional shear strains

$$e_a{}^R = \frac{1}{K_{11}} e_a{}^I - \frac{K_{12}}{K_{11}} \gamma_1{}^R - \frac{K_{13}}{K_{11}} \gamma_2{}^R \quad \text{(C3)}$$

Acknowledgments. This work was performed with support from the U.S. Geological Survey, Department of the Interior, under the National Earthquake Hazards Reduction Program. Contents do not represent policy of that agency, and no endorsement of the agency is to be assumed. The borehole tensor strain instrument was previously developed under awards of the Australian Research Grants Scheme. We thank R. Liechti for significant contributions to maintaining the continuity of the borehole strain meter record, A. Linde for useful discussions on tidal calibration of borehole strain meters, and M. Eva and staff of the Dorothy Hill Geology Library for effective support. The manuscript has benefited from helpful reviews by S. Hickman, J. Langbein, and E. Roeloffs. The operation of the borehole strain meters is made possible by careful and dedicated work from technical staff of the Physics Department, University of Queensland.

References

Agnew, D. C., Strain tides at Pinon Flat: Analysis and interpretation, Ph.D. thesis, Univ. of Calif., San Diego, La Jolla, 1979.

Agnew, D. C., Strainmeters and tiltmeters, *Rev. Geophys.*, *24*, 579-624, 1986.

Amadei, B., *Rock Anisotropy and the Theory of Stress Measurements*, Springer-Verlag, New York, 1983.

Baker, T. F., Methods of tidal loading computation, *Mar. Terr.*, *94*, 6365-6372, 1985.

Beaumont, C., Tidal loading: Crustal structure of Nova Scotia and the M2 tide in the northwest Atlantic from tilt and gravity observations, *Geophys. J. R. Astron. Soc.*, *53*, 27-53, 1978.

Beaumont, C., and J. Berger, An analysis of tidal strain observations from the United States of America, I, The homogeneous tide, *Bull. Seismol. Soc. Am.*, *65*, 1613-1629, 1975.

Berger, J., and C. Beaumont, An analysis of tidal strain observations from the United States, II, The inhomogeneous tide, *Bull. Seismol. Soc. Am.*, *66*, 1821-1846, 1976.

Crampin, S., Geological and industrial implications of extensive-dilatency anisotropy, *Nature*, *328*, 491-496, 1987.

Desai, C. S., and J. F. Abel, *Introduction to the Finite Element Method: A Numerical Method for Engineering Analysis*, Van Nostrand Reinhold, New York, 1971.

Du, Y., P. Segall, and H. Gao, Dislocations in inhomogeneous media via a moduli perturbation approach: General formulation and two-dimensional solutions, *J. Geophys. Res.*, *99*, 13767-13779, 1994.

Evans, K. and F. Wyatt, Water table effects on the measurement of Earth strain, *Tectonophysics*, *108*, 323-337, 1984.

Evans, R., J. Beavan, R. Bilham, and G. King, A survey of Earth strain tides in Great Britain, *Geophys. J. R. Astron. Soc.*, *57*, 119-135, 1979.

Frank, F. C., Deduction of Earth strains from survey data, *Bull. Seismol. Soc. Am.*, *56*, 35-42, 1966.

Gladwin, M. T., High precision multi component borehole deformation monitoring, *Rev. Sci. Instrum.*, *55*, 2011-2016, 1984.

Gladwin, M. T., and R. Hart, Design parameters for borehole strain instrumentation, *Pure Appl. Geophys.*, *123*, 59-80, 1985.

Gladwin, M. T., R. L. Gwyther and R. Hart, Tidal calibration of borehole vector strain instruments (abstract), *Eos Trans. AGU*, *66*, 1057, 1985.

Harrison, J. C., Cavity and topographic effects in tilt and strain measurements, *J. Geophys. Res.*, *81*, 319-328, 1976.

Harrison, J. C., *Earth Tides*, Van Nostrand Reinhold, New York, 1985.

Hart, R. H. G., Developments in calibration and inhomogeneous modelling for borehole strain instruments: Improved constraints on fault slip parameters, Ph.D. thesis, Univ. of Queensland, Queensland, Australia, 1996.

Hu, G., W. Menke, and C. Powell, Polarization tomography for *P* wave velocity structure in southern California, *J. Geophys. Res.*, *99*, 15245-15256, 1994.

Hudnut, K., et al., Coseismic deformations in the Landers earthquake sequence, *Bull. Seismol. Soc. Am.*, *84*, 625-645, 1994.

Humphreys, E. D., and R. W. Clayton, Tomographic image of the southern California mantle, *J. Geophys. Res.*, *95*, 19725-19746, 1990.

Humphreys, E. D., and K. G. Dueker, Western U.S. upper mantle structure, *J. Geophys. Res.*, *99*, 9615-9634, 1994.

Ishiguro, M., and Y. Tamura, BAYTAP-G in TIMSAC-84, *Comput. Sci. Monogr.*, *22*, 56-117, 1985.

Jaeger, J. C., and N. G. W. Cook, *Fundamentals of Rock Mechanics*, Chapman and Hall, New York, 1976.

Johnston, M., A.T. Linde, M.T. Gladwin, and R. Borcherdt, Fault failure with moderate earthquakes, *Tectonophysics*, *144*, 189-206, 1987.

King, G., W. Zurn, R. Evans, and D. Emter, Site correction for long period seismometers, tiltmeters and strainmeters, *Geophys. J. R. Astron. Soc.*, *44*, 405-411, 1976.

Kohl, M., and J. Levine, Using a short baseline borehole tiltmeter to measure the regional tilt (abstract), *Eos Trans. AGU*, *73*(43), Fall Meet. Suppl., 121, 1992.

Kohl, M. L., and J. Levine, Measuring low frequency tilts, *J. Res. Natl. Inst. Stand. Technol.*, *98*, 191-202, 1993.

Leary, P. C., S. Crampin, and T. V. McEvilly, Seismic fracture anisotropy in the Earth's crust: An overview, *J. Geophys. Res.*, *95*, 11105-11114, 1990.

Linde, A. T., and M. J. S. Johnston, Source parameters of the October 1, 1987, Whittier Narrows earthquake from crustal deformation data, *J. Geophys. Res.*, *94*, 9633-9643, 1989.

Mao, W. J., Loading tides on a stratified viscoelastic self-gravitating half-space, *Geophys. J. Int.*, *102*, 537-550, 1990.

Monaghan, A. J., The effects of rock anisotropy on borehole strain measurements, honours thesis, Univ. of Queensland, Queensland, Australia, 1990.

Mooney, W. D., Seismic methods for determining earthquake source parameters and lithospheric structure, in *Geophysical Framework of the Continental United States*, edited by L. C. Pakiser and W. D. Mooney, *Mem. Geol. Soc. Am., 172*, 11-34, 1989.

Mooney, W. D., and C. S. Weaver, Regional crustal structure and tectonics of the Pacific Coastal States; California, Oregon, and Washington, in *Geophysical Framework of the Continental United States*, edited by L. C. Pakiser and W. D. Mooney, *Mem. Geol. Soc. Am., 172*, 129-161, 1989.

Roeloffs, E. A., S. Burford, F. S. Riley, and A. W. Records, Hydrologic effects on water level changes associated with episodic fault creep near Parkfield, California, *J. Geophys. Res., 94*, 12387-12402, 1989.

Sacks, I. S., S. Suyehiro, D. W. Evertson, and Y. Yamagishi, Sacks-Evertson strainmeter, its installation in Japan and some preliminary results concerning strain steps, *Pap. Meteorol. Geophys., 22*, 195-207, 1971.

Sakata, S., and H. Sato, Borehole-type tiltmeter and three-component strainmeter for earthquake prediction, *J. Phys. Earth, 34*, suppl., S129-S140, 1986.

Sato, T., and H. Hanada, A program for the computation of oceanic tidal loading effects 'GOTIC', *Publ. Int. Latt. Obs. Mizusawa, 18*, 29-47, 1984.

Sato, T., and J. C. Harrison, Local effects on tidal strain measurements at Esashi, Japan, *Geophys. J. Int.*, 102, 513-526, 1990.

Scherneck, H.-G., A parametrized solid earth tide model and ocean tide loading effects for global geodetic baseline measurements, *Geophys. J. Int., 106*, 677-694, 1991.

Schwiderski, E. W., On charting global ocean tides, *Rev. Geophys., 18*, 243-268, 1980.

Shimada, S., S. Sakata, and S. Noguchi, Coseismic strain steps observed by three-component borehole strainmeters, *Tectonophysics, 144*, 207-214, 1987.

Stefansson, R., I. S. Sacks, and A. T. Linde, Calibration of borehole strainmeters, *Year Book Carnegie Inst. Washington, 80*, 570-572, 1981.

Stock, G., Modelling of tides and tidal dissipation in the Gulf of California, Ph.D. thesis, Univ. of Calif., San Diego, 1976.

Wahr, J., Body tides on an elliptical, rotating, elastic and oceanless Earth, *Geophys. J. R. Astron. Soc., 64*, 677-703, 1981.

Wyatt, F. K., Measurements of coseismic deformation in southern California: 1972-1982, *J. Geophys. Res., 93*, 7923-7942, 1988.

Wyatt, F. K., Displacement of surface monuments: Vertical motion, *J. Geophys. Res., 84*, 1655-1664, 1989.

Wyatt, F. K., D. C. Agnew, and M. T. Gladwin, Continuous measurements of crustal deformation for the 1992 Landers earthquake sequence, *Bull. Seismol. Soc. Am., 84*, 768-779, 1994.

D. C. Agnew and F. K. Wyatt, Institute of Geophysics and Planetary Physics, University of California, San Diego, La Jolla, CA 92093-0225. (e-mail: agnew@ramsden.ucsd.edu; wyatt@ramsden.ucsd.edu)

M. T. Gladwin, R. L. Gwyther, and R. H. G. Hart, Division of Exploration and Mining, CSIRO, P.O. Box 883, Kenmore, Queensland, Australia, 4069. (e-mail: m.gladwin@dem.csiro.au; r.gwyther@dem.csiro.au; r.hart@dem.csiro.au)

(Received November 1, 1995; revised July 8, 1996; accepted July 18, 1996.)